Assessing CryoSat-2 Antarctic snow freeboard retrievals using data from ICESat-2

S. W. Fons[1,2], N. T. Kurtz[2], M. Bagnardi[2,3], A. A. Petty[2,4], and R. L. Tilling[2,4]

[1]Department of Atmospheric and Oceanic Science, University of Maryland, College Park, MD, USA

[2]Cryospheric Sciences Laboratory, NASA Goddard Space Flight Center, Greenbelt, MD, USA

[3]ADNET Systems, Inc., Bethesda, MD, USA

[4]Earth System Science Interdisciplinary Center, University of Maryland, College Park, MD, USA

Corresponding author: Steven W. Fons (steven.w.fons@nasa.gov)

Key Points:

- We present an updated CryoSat-2 Antarctic snow freeboard retrieval method
- These improved CryoSat-2 snow freeboard retrievals show strong agreement with ICESat-2 data both along-track and basin-wide

Abstract

NASA's Ice, Cloud, and land Elevation Satellite-2 (ICESat-2) laser altimeter launched in Fall 2018, providing an invaluable addition to the polar altimetry record generated by ESA's CryoSat-2 radar altimeter. The simultaneous operation of these two satellite altimeters enables unique comparison studies of sea ice altimetry, utilizing the different frequencies and profiling strategies of the two instruments. Here, we use freeboard data from ICESat-2 to assess Antarctic snow freeboard retrievals from CryoSat-2. We first discuss updates made to a previously-published CryoSat-2 retrieval process and show how this Version 2 algorithm improves upon the original method by comparing the new retrievals to ICESat-2 in specific along-track profiles as well as on the basin-scale. In two near-coincident along-track profiles, we find mean snow freeboard differences (standard deviations of differences) of 0.3 (9.3) and 7.6 cm (9.6 cm) with 25 km binned correlation coefficients of 0.77 and 0.89. Monthly mean freeboard differences range between -2.9 (10.8) and 6.6 cm (16.8 cm) basin wide, with the largest differences typically occurring in Austral fall months that is hypothesized to be related to new ice growth and the use of static snow backscatter coefficients in the retrieval. Monthly mean correlation coefficients range between 0.57 and 0.80. While coincident data show good agreement between the two sensors, they highlight issues related to geometric and frequency sampling differences that can impact the freeboard distributions.

Plain Language Summary

Measuring sea ice freeboard from space is an important first step in estimating its thickness. A previous study had developed a new method of measuring freeboard over Antarctic sea ice using ESA's CryoSat-2 altimeter, however, few validation data existed at the time to determine how well it performed. In this paper, we improve the CryoSat-2 processing and make use of data from NASA's ICESat-2 altimeter for comparisons with the CryoSat-2 data. While agreement is strong overall, there are still differences between the measurements that we hypothesize come from the different footprint sizes and wavelengths of the two instruments.

1 Introduction

ESA's CryoSat-2 radar altimeter has provided a more than 10-year time series of surface elevation data since its launch in 2010 that has been invaluable for cryospheric studies. For sea ice research in particular, CryoSat-2 has enabled basin-scale estimates of Arctic sea ice freeboard and thickness from space, building on the satellite altimeter-based freeboard/thickness time series that began with ERS-1 and -2 (Laxon et al., 2003) and continued with ICESat (Zwally et al., 2008) and Envisat (Connor et al., 2009). Freeboard data from CryoSat-2 have been used to quantify Arctic sea ice thickness and volume over time (Kwok & Cunningham, 2015; Laxon et al., 2013; Tilling et al., 2018), to develop new retrieval algorithms for sea ice properties (Kurtz et al., 2014; Lee et al., 2016), and to better understand potential bias and uncertainty from radar altimetric studies of sea ice (Kwok 2014; Landy et al., 2020; Nandan et al., 2017; Ricker et al., 2014).

Despite its widespread use in the Arctic, CryoSat-2 data remain underutilized for sea ice research in the Southern Ocean (Meredith et al., 2019). This is due primarily to the contrast between the Arctic and Antarctic snow layer that affects radar altimetry. Also, the lack of available pan-Antarctic snow depth on sea ice information contributes to the uncertainty in the

dominant scattering horizon from radar returns and limits accurate sea ice freeboard and thickness retrievals (Massom et al., 2001; Paul et al., 2018). Nevertheless, some studies have attempted to provide estimates of freeboard and thickness using different methods and with various caveats. Kwok and Kacimi (2018) calculated ice freeboard and thickness profiles in the Weddell Sea using CryoSat-2 and data from NASA's Operation IceBridge (OIB). Snow depth values were estimated by subtracting the CryoSat-2 freeboards from the Airborne Topographic Mapper (ATM) laser (total) freeboards. Price et al. (2015) similarly computed thickness from CryoSat-2 in a single region – McMurdo Sound – using snow depth from models, reanalysis, and passive microwave sensors. Work done through ESA's sea ice Climate Change Initiative (CCI, Paul et al., 2018; Schwegmann et al., 2016) showcased freeboard retrievals in the Southern Ocean and comparisons between CryoSat-2 and Envisat, but uncertainties in the Ku-band retrievals stemming from the snow layer on Antarctic sea ice allowed only for "experimental" thickness estimates (Hendricks et al., 2018). Fons and Kurtz (2019) put forth a waveform-fitting method that attempted to circumvent the complexities of the effect of the snow layer on radar returns by retrieving the air-snow interface elevation from CryoSat-2. This work exploited the fact that scattering at Ku-band frequencies – though potentially smaller in magnitude than scattering from the snow-ice interface – does occur from the air-snow interface (Kwok 2014; Willatt et al., 2010), and incorporated this scattering in a forward waveform model. While the results showed promise, they lacked independent, pan-Antarctic snow freeboard data to validate the retrievals.

While challenges to CryoSat-2-derived Antarctic sea ice freeboard and thickness remain, studies using satellite laser altimetry have proven more successful. Laser altimeters range to the surface of the snow on sea ice and therefore are not impacted by the uncertain scattering horizon within the snow layer. The freeboard retrieved from laser altimeters is therefore the snow freeboard, which can be combined with snow depth information to estimate thickness. NASA's ICESat was the main platform used for laser altimetric studies of sea ice prior to 2019, and studies combined the retrieved snow freeboard with snow depth information from various sources, including passive microwave-derived snow depth (Zwally et al., 2008), a zero-ice-freeboard assumption (Kurtz & Markus, 2012), and a one-layer modified density model (Kern et al., 2016, Li et al., 2018) to compute thickness. The launch of ICESat-2 in late 2018 has provided an opportunity to advance sea ice research in the Southern Ocean, both in stand-alone studies of Antarctic sea ice and as a unique compliment to CryoSat-2 for combination studies and validation. One such study (Kacimi & Kwok, 2020) combined CryoSat-2 radar freeboards with ICESat-2 snow freeboards to make estimates of snow depth on Antarctic sea ice. They used the resulting snow depth and freeboards to estimate pan-Antarctic thickness and volume for the Austral winter 2019. These results showcase a new thickness dataset but are limited to the years in which both satellites are operating. More combination studies are possible if the recent CRYO2ICE campaign (ESA, 2018), which better aligned the CryoSat-2 orbit with that of ICESat-2 to improve spatial/temporal coincidence in the Arctic, is altered to optimize the orbital overlaps in the Southern Hemisphere.

Here, we utilize ICESat-2 Southern Ocean snow freeboard data to validate the CryoSat-2 snow freeboard retrieval method originally published in Fons and Kurtz (2019). Fons and Kurtz (2019) was a feasibility study that lacked coincident validation data for proper evaluation. Now, with ICESat-2, we are able to better assess and draw conclusions on the CryoSat-2 freeboard retrievals. This work will first discuss improvements made to the CryoSat-2 retrieval algorithm since publication in 2019, which include updates to the model parameters, sea surface height

(SSH) determination, the sea ice surface height pdf, and other components of the algorithm (section 3). Then, we showcase validation of the improved algorithm using data from ICESat-2 both along-track and pan-Antarctic (section 4). We conclude with a discussion of potential error sources, sampling biases, and difficulties of laser-radar comparisons (sections 5 and 6). Overall, this assessment adds more confidence to the CryoSat-2 results, which could enable snow freeboard retrievals from the entire mission (2010-present) and provide a step towards Antarctic snow depth and sea ice thickness estimates through the waveform fitting of CryoSat-2 returns.

2 Data

The primary dataset used in this work is the CryoSat-2 baseline-D Level 1-B waveform data (ESA 2019, ESA 2019a). These data are acquired by the SIRAL instrument aboard CryoSat-2, which has a frequency in the Ku-band centered at 13.575 GHz (Wingham et al., 2006). SIRAL operates in three different modes: low resolution mode (LRM), synthetic aperture mode (SAR), and synthetic aperture-interferometric mode (SARIn). Both the SAR and SARIn modes are utilized in this study and provide complete coverage of the Antarctic sea ice pack. The CryoSat-2 echoes in SAR and SARIn modes represent a pulse-doppler-limited footprint of approximately 380 m along track and 1.65 km across track (ESA, 2019b; Scagliola, 2013), however, these echoes can be influenced by off-nadir, specular returns from approximately 15 km across-track (Tilling et al., 2018). For consistency, both SAR and SARIn waveforms are reduced to 128 range bins, with SAR data being truncated and SARIn data being clipped to 128 range bins about the maximum power location. We compute elevation from these waveforms following the procedure outlined in Fons and Kurtz (2019), which involves retracking the waveforms and applying the geophysical and retracking corrections to the raw ranges.

To assess the retrieved CryoSat-2 snow freeboards we utilize snow freeboard data from ICESat-2, specifically, the release 3 Level 3A sea ice freeboard product ATL10 (Kwok et al. 2020). ATL10 provides estimates of snow freeboard in both hemispheres for each of the six ICESat-2 beams. The freeboard estimates are computed using the sea ice and sea surface elevations from the ATL07 sea ice height product, which includes variable length segments (ranging from ~20-200 m) encompassing 150 returned signal photons (Kwok et al., 2019, 2020a). Here, we use the highest resolution, segment-scale “beam freeboard”, which provides a freeboard estimate for each beam and ATL07 segment using only the leads estimated along the given beam (Kwok et al., 2020a). Only the three strong beams are used in this study as they provide a higher along-track resolution than the weak beams (Kwok et al., 2019). Unless otherwise noted, mentions of “freeboard” in this paper refer to the snow freeboard (i.e. the height of the sea ice and snow above the sea surface).

For this study, the CryoSat-2 and ICESat-2 data are analyzed for the coincident ICESat-2 overlap period, ranging from October 2018 until October 2020. Pan-Antarctic maps of freeboard are computed using monthly means and gridded to the NSIDC 25 km x 25 km polar stereographic grid. CryoSat-2 snow freeboards below -0.1 m and above 3.0 m are filtered out prior to gridding, to account for instrument noise and to remove anomalously high freeboard values. Gridded values are only computed if the grid cell contains at least five samples and an ice concentration of at least 50%. We use Version 3 Bootstrap monthly average ice concentration data (Comiso, 2017) for 2018 and 2019, and use the NOAA/NSIDC Climate Data Record Near-Real-Time (NRT CDR) monthly sea ice concentration product for 2020, when the Bootstrap data are not yet available (Meier et al., 2017). The NRT CDR product essentially takes the higher

151 value from the Bootstrap and NASA Team algorithms (Cavalieri et al., 1997). ICESat freeboard
152 data are used in a limited capacity in this work (described in section 3.1) as part of an
153 initialization of the waveform-fitting model. These data range from 2003-2008, with a
154 description found in Kurtz and Markus (2012).

155 **3 Algorithm design and improvements**

156 In this section, we provide a brief overview of the procedure put forth in Fons and Kurtz
157 (2019), which herein will be referred to as Version 1 (V1), but focus mainly on the
158 improvements that have been made to the algorithm to create Version 2 (V2). For a more
159 detailed look at the model and waveform-fitting process, see Fons and Kurtz (2019).
160 To retrieve sea ice elevation and calculate freeboard from CryoSat-2, we employ a
161 physical – as opposed to the more commonly used empirical – retracking technique. This
162 technique uses a forward model and waveform-fitting algorithm that constructs a modeled
163 CryoSat-2 waveform from given initial parameters, fits the model to the CryoSat-2 data using an
164 optimization approach, and calculates the retrieved elevation using the best-fit waveform and
165 parameters. The output (free) parameters are given in Table S1, where the snow depth and snow-
166 ice interface time delay allow us to compute the elevations of both the air-snow and snow-ice
167 interfaces, and from there, estimate both the snow freeboard and the ice freeboard. The initial
168 guess parameters in Table S1 are derived from the actual CryoSat-2 waveform and independent
169 measurements. This method was originally put forth in Kurtz et al. (2014), and then was
170 modified to include scattering effects from the snow layer in Fons and Kurtz (2019). In the V1
171 retrieval, the modeled waveform was given by:
172
173 $$\Psi(\tau) = P_t(\tau) \otimes I(\tau, \alpha) \otimes p(\tau, \sigma) \otimes \nu(\tau, h_{sd}) \quad (1)$$
174
175 where Ψ is the constructed waveform, P_t is the transmit pulse, I is the rough surface impulse
176 response, p is the surface height probability density function, and ν is the scattering cross section
177 per unit volume – all of which are a function of τ, the echo delay time on the waveform, and
178 other parameters given in Table S1 (Fons & Kurtz, 2019; Kurtz et al., 2014). Since Fons and
179 Kurtz (2019), we have improved a few aspects of the original method to better model sea ice
180 waveforms and reduce the potential for convergence on local minima, resulting in the V2
181 algorithm. The main improvements consist of: reducing the number of free parameters in the
182 model, using a new surface height probability density function (pdf), altering the SSH
183 calculation, and a few smaller modifications. These changes are explained in this section.
184

185 **3.1 Free parameters**

186 The V1 algorithm used a model with nine free parameters – a relatively large number that
187 increases the potential for the waveform-fitting optimization procedure to converge on a local, as
188 opposed to global, minimum. In V2, we elected to reduce the number to five parameters and
189 designated the radar backscatter terms of snow and ice as static. Given the uncertainty associated
190 with these backscatter parameters, we now rely on values published previously (given in Table
191 S1). We make the assumption that these static terms represent average values across the
192 Antarctic, and acknowledge that further study into these quantities could provide useful
193 information on their seasonal and regional variations. V1 retrievals used ICESat data as an initial
194 guess for the air-snow interface location parameter. In V2, we have updated the free parameter to

be physically quantifiable (snow depth) and are instead using a combined ICESat and ICESat-2 monthly "climatology" as the initial guess. Like in V1, we invoke the 'zero ice freeboard' assumption for this initial guess that assumes the snow depth is equal to the snow freeboard (the implications for this assumption are discussed in section 3.5). Each monthly climatology initialization map (12 in total, one for each month) consists of multiple years of ICESat and ICESat-2 snow freeboard data from the given month averaged together. The ICESat data for a given month comes from the years 2003-2008, while the ICESat-2 data for that month comes from the years 2018-2019. We added ICESat-2 data to the initialization to incorporate more – and more recent – data into the initial guess. Additionally, ICESat only collected data during a few months each year while ICESat-2 collects data year round. The added ICESat-2 data therefore provide month-to-month variability in the initial guess. By creating this monthly climatology, we use the same, independent, consistent initialization from year to year. The free parameters used here are given in Table S1.

3.2 Surface height pdf

In the V1 algorithm, a zero-mean Gaussian distribution was used to represent the surface height pdf in the waveform model. Here in V2, we have updated the surface height pdf to be a lognormal distribution, which has been shown (over Arctic sea ice) to better represent the sea ice surface pdf over CryoSat-2 footprint scales (Landy et al., 2020) . This distribution is given as:

$$p(\tau) = \frac{1}{\tau\sigma_l\sqrt{2\pi}} \exp\left(-\frac{(ln\,\tau-\mu)^2}{2\sigma_l^2}\right) \quad (2)$$

where μ and σ_l represent the mean and standard deviation, respectively, of the natural logarithm of the surface height. We assume a zero-mean distribution and initialize the roughness term (σ) as 0.15, which gets converted to σ_l and adjusted during fitting as a free parameter. The impact of the lognormal surface height pdf is shown in Figure 1. Modeled waveforms were created with varying roughness values and run using both a lognormal (solid) and normal (dashed) surface height pdf. For small roughness values, the difference in the modelled waveform shape (measured by the squared norm of the residuals) when using the lognormal versus normal distribution is negligible. Conversely, as the roughness increases, these differences increase exponentially. Judging by the example roughness distribution output by this algorithm from September 2020 (Figure 1), most fit waveforms have σ values between 0.1 and 0.45 m and therefore are less sensitive to the modified surface height pdf used. However, there are still waveforms fit with σ values over 0.5 m which would be more sensitive to the modified surface height pdf and benefit from the more representative lognormal distribution.

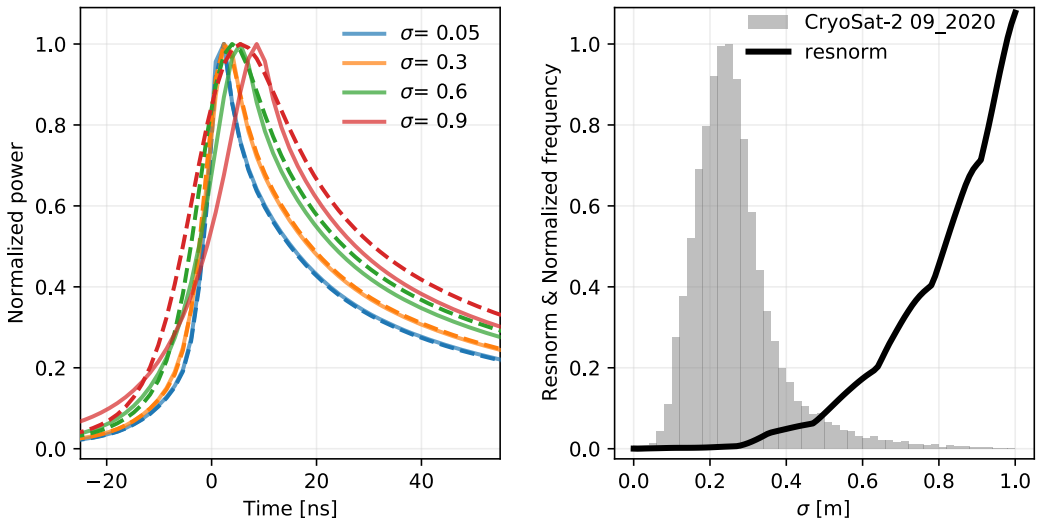

Figure 1. Sensitivity of modelled waveform shape to roughness and surface height pdf used. Left: Solid lines show modelled waveforms with varying values of σ created using a lognormal surface height pdf, while dashed lines show the same but using a normal surface height pdf. Right: The difference in shape is quantified using the squared norm of the residual (resnorm, black line) plotted at 1 cm increments from 0 to 1 m roughness. An example normalized histogram of gridded σ values from September 2020 is shown to give its expected range.

3.3 Sea surface height

The SSH determined by lead elevations in V1 was, in essence, a 25 km gridded SSH. Though freeboard was computed along-track, the sea surface was averaged for all tracks within the grid cell, and then subtracted from the along-track sea ice elevations. This method overlooked the smaller scale variability in SSH, and therefore potentially biased our retrievals. In V2, we instead calculate an along-track SSH. Following Kwok and Cunningham 2015, we average all the lead-type elevations in along-track segments, and discard any segments where fewer than three SSH measurements exist. Given that the lead distribution within the Antarctic sea ice pack is more widespread than that of Arctic sea ice (Reiser et al., 2020), we use a segment length of 10 km as opposed to 25 km in Kwok and Cunningham 2015. The 10 km SSH segment length is the same as that used in the ICESat-2 along-track sea ice data products (Kwok et al., 2020).

3.4 Additional modifications

In addition to the improvements mentioned above, a few smaller changes were made to improve on the V1 retrievals and streamline the processing. For one, we implemented an “ocean” surface type classification in V2 using the waveform characteristics of stack standard deviation (SSD) and skewness. Waveforms with an SSD greater than 50, a skewness less than 0.3, and an along-track rolling average of skewness less than 0.3 are considered ocean points and filtered out before fitting. The rolling average is used to invoke a more conservative filtering scheme, so that single returns with an anomalously low skewness would not be misclassified as ocean-type and so that the sea ice edge would be preserved for fitting and later potential filtering due to ice concentration (Figure S1).

Another update to V1 was made to the radar propagation correction that accounts for scattering within the snowpack. The V1 algorithm used a typical representation of this correction, given by:

$$\delta h = Z_r(1 - c_s/c) \quad (3)$$

where δh is the radar range correction, c is the radar wave speed, c_s is the wave speed through snow, and Z_r is the snow depth corrected for wave speed (Mallett et al., 2020). However, the V1 algorithm treated Z_r as the actual snow depth (as it is conventionally interpreted, Mallett et al., 2020) when it should have been corrected for wave speed through snow. Mallett et al. (2020) showed that this interpretation can lead to a bias in the freeboard retrievals through the erroneous reduction by a factor of c_s/c. In the V2 algorithm, we correct this interpretation and instead use the wave-speed-corrected snow depth in equation 3, given by:

$$Z_r = Z\,(c/c_s) \quad (4)$$

where Z is the real snow depth.

The last update made involved converting the processing from MATLAB to Python programming language. While care was taken to ensure that results were consistent between the two languages, inherent differences in the standard curve fitting toolboxes led to small discrepancies from V1 to V2. For best consistency with the previous processing, we utilize the scipy curve_fit package (Virtanen et al., 2020) over other fitting packages.

3.5 Retrieval assumptions and limitations

Despite the improvements made to create the V2 algorithm, certain assumptions are still inherent within the freeboard retrievals that could impact results. One such assumption is the zero ice freeboard assumption used to initialize the snow depth parameter. We invoke this assumption when inputting the snow freeboard climatology as a first guess for snow depth. It is understood that while the zero-ice freeboard can be a good assumption is some regions and seasons (Kurtz & Markus, 2012), it is likely not valid for the whole Antarctic sea ice pack (Kwok & Kacimi, 2018) and may lead to biases in the retrievals (discussion in section 5). It is used as a starting point until better snow depth information is available.

Another limitation of the model is its handling of surface roughness. Roughness at different length scales has been shown to significantly impact Ku-band radar returns and bias freeboard retrievals (Landy et al., 2020). We attempt to handle this fact by setting σ as a free parameter in the model, with bounds that cover the expected range of roughness (0-1 m). However, the tracking point on a radar waveform can be influenced by roughness (Figure 1, Landy et al., 2020), and therefore our single-value initialization for snow-ice interface tracking point (t) may introduce a bias. Further work is needed to determine the impacts of a roughness-induced dynamic tracking point initialization on elevation and freeboard retrievals using this method.

4 Results

We processed all CryoSat-2 data from October 2018 to October 2020 using the V2 algorithm processing. This section compares the retrieved CryoSat-2 snow freeboards to those from ICESat-2 by examining along-track retrievals using near-contemporaneous overlaps of the

two satellites (section 4.1) and comparing pan-Antarctic, monthly gridded freeboard data (section 4.2). Variability in the snow freeboard retrievals is shown in section 4.3, while potential sources for Austral fall differences are discussed in section 4.4.

4.1 Along-track comparisons

To compare the freeboard retrieval performance along-track, we first found near-contemporaneous overlaps in the two satellites' ground tracks that occurred in the sea ice zone with the least possible time difference. We define an orbital overlap as a CryoSat-2 and ICESat-2 ground track being within 4 km of each other for at least 10 seconds of flight time, which is approximately 70 km along-track. Given the 1.65 km across-track footprint of CryoSat-2 and the 3.3 km spread of the three beam pairs of ICESat-2, 4 km is the maximum separation that could still theoretically result in overlapping footprints. We find that this overlap definition results in reasonably overlapping orbital tracks for freeboard comparisons. When the maximum allowable time difference was restricted to 5 hours, 179 such overlaps occurred in various lengths and locations around the Southern Ocean between October 2018 and October 2020 (Figure 2). It is important to note that, with the definition above, no such overlaps have occurred in the Southern Hemisphere sea ice zone since the CRYO2ICE orbit re-configuration – which was optimized for Arctic overlaps – took place in late July 2020.

Due to the orbital alignments and distance of the sea ice pack from the pole (where orbit density is greater), none of the 179 overlaps have occurred with less than three hours of time difference, which is expected for overlaps lasting longer than five seconds (ESA, 2018, slide 14). All overlaps occurred with between 3.0 and 4.2 hours difference and lasted between ~70 km and ~1800 km. These overlaps come from the satellite orbits alone and do not take into account available freeboard data. Therefore, despite the large number of overlaps (Figure 2), many are not ideal for comparisons due to their short length (for those occurring in regions of smaller ice extent) or missing freeboard data (mostly from ICESat-2 missing data due to clouds). Here, we have chosen two Austral winter overlaps with many available ICESat-2 data: 27 October 2018, when the satellite ground tracks were approximately 4 hours and 10 minutes apart, and 02 September 2019, when they were about 3 hours and 36 minutes apart (Figure 3). Both overlaps were close to 1015 km long over the sea ice zone, but were trimmed to 1000 km (2018) and 800 km (2019) to remove end sections of the overlaps where significant amounts of ICESat-2 data were missing. Implications of the time differences are discussed in section 5.

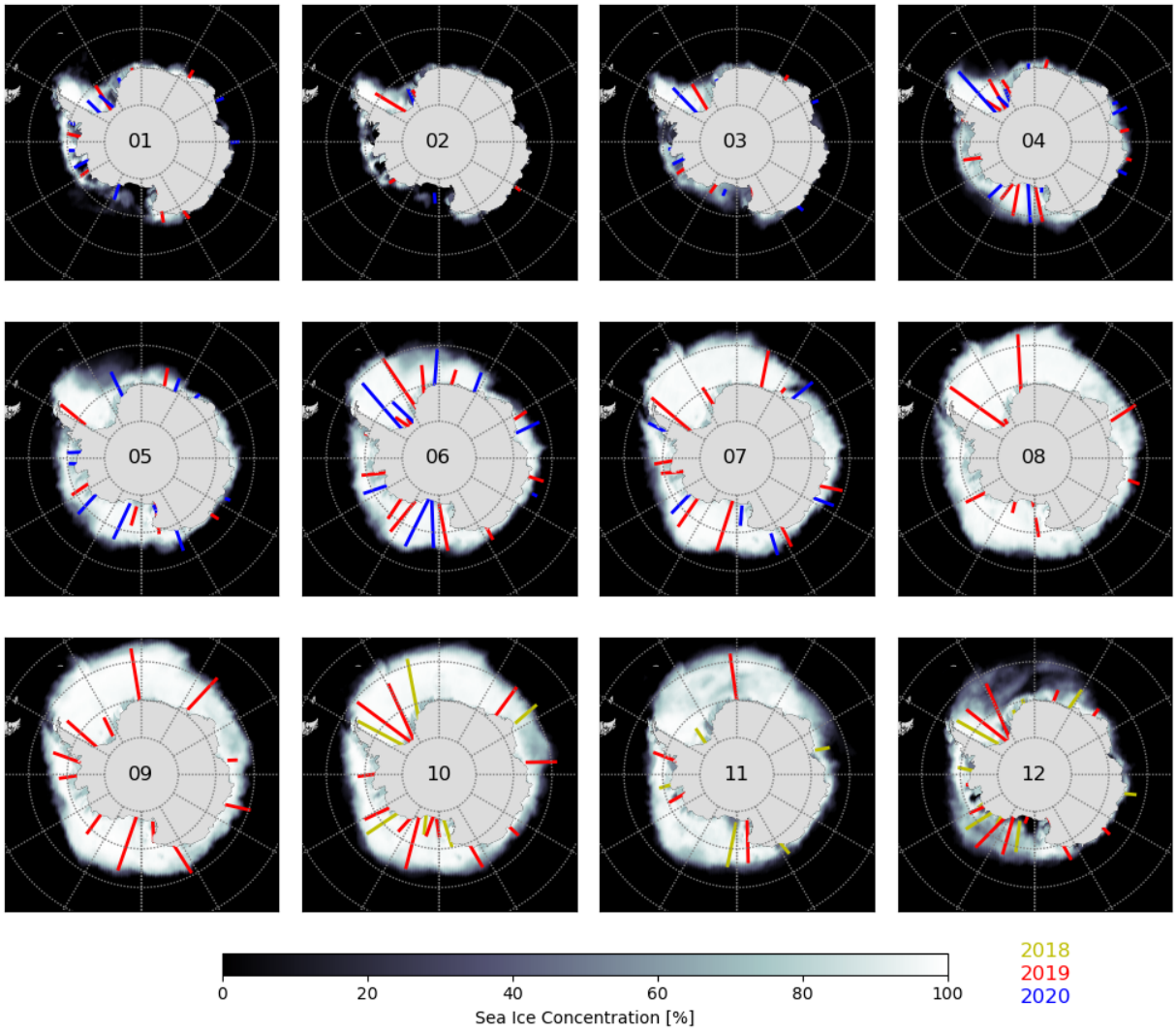

Figure 2. CryoSat-2 and ICESat-2 orbit overlaps (defined in text) from October 2018 to December 2020, colored by year. Sea ice concentrations for each month are averages of the years in which there are overlaps present.

Figure 3 shows the two along-track comparisons of snow freeboard between CryoSat-2 and ICESat-2. Both the shot-to-shot and 25 km binned average freeboards are shown. In the 2018 (2019) profile, the mean difference is 0.3 cm (7.6 cm) and the standard deviation of differences is 9.3 cm (9.6 cm). Though the 25 km binned correlation is higher in 2019 (0.89) than in 2018 (0.77), the distribution captured by CryoSat-2 in 2018 tends to match ICESat-2 better than in 2019. There is a clear discrepancy in the number of data points from each sensor, with ICESat-2 recording 120-140 times more valid measurements than CryoSat-2. This discrepancy is largely due to the footprint size difference: the smaller footprint of ICESat-2 allows for many more measurements over a given distance than CryoSat-2. Additionally, some

CryoSat-2 data are filtered out due to leads (to which CryoSat-2 is more sensitive), mixed surface returns, or poor fitting, which further reduces the number of valid measurements.

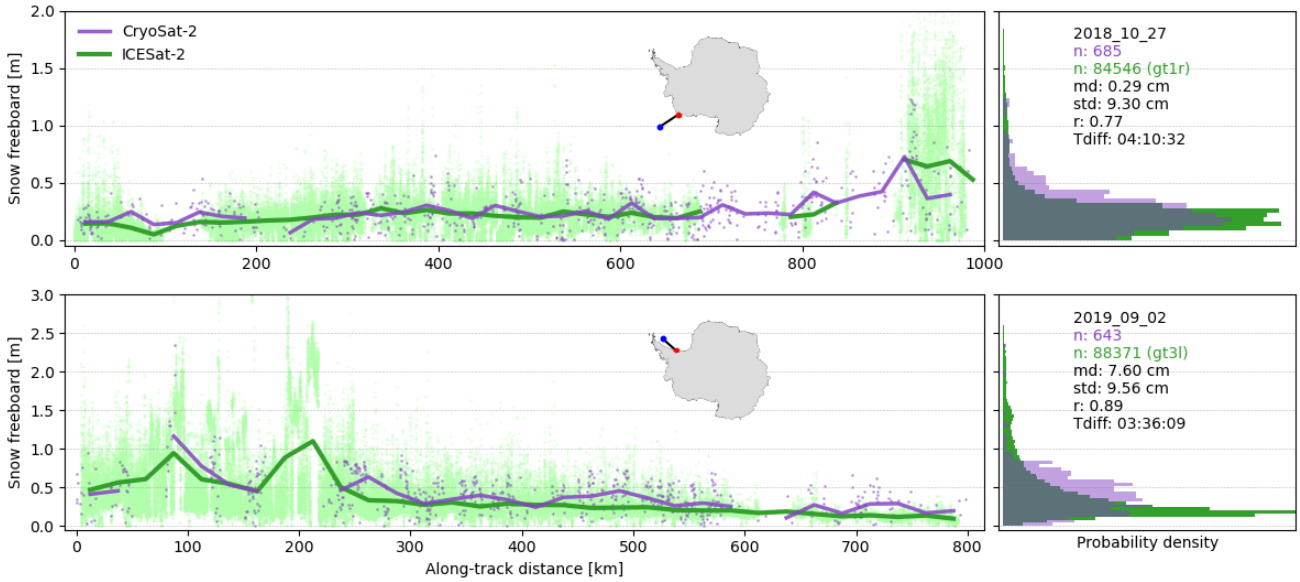

Figure 3. Along-track comparisons from two near-coincident overlaps of ICESat-2 (green) and CryoSat-2 (purple). Both profiles showcase data from the CryoSat-2 V2 algorithm. Points show individual measurements while lines give a binned 25 km average. ICESat-2 data come from a single strong beam, given in the right plots. Binned averages are only computed if at least 5% of the possible datapoints for that bin exist. Mean differences (md), standard deviations of differences (std) and correlation coefficients (r) are given in the right plots. Maps show the overlaps used in the profile, with the blue point representing the start and red point representing the end of the profile.

4.2 Monthly gridded comparisons

The V2 retrieval algorithm was applied to all CryoSat-2 data within the ICESat-2 era, and monthly gridded maps of snow freeboard were created. Figure 4 shows an example monthly map (September 2020) of CryoSat-2 V2 data in comparison with that from ICESat-2 and CryoSat-2 V1. As mentioned in section 3.1, only ICESat-2 data from 2018 and 2019 were used in the initialization climatology. Therefore, none of the 2020 ICESat-2 data were included in the initialization of the CryoSat-2 model, allowing for independent monthly comparisons. Snow freeboard values ranged from nearly 0 to over 1.8 m, with a mean (mode) value of 28 cm (21 cm) from CryoSat-2 and 29 cm (23 cm) from ICESat-2. The pan-Antarctic map of freeboard matches well between the two sensors, as the widespread patterns found with ICESat-2 are captured by the CryoSat-2 retrievals with a correlation coefficient of 0.77. A majority of the differences between CryoSat-2 and ICESat-2 are within +/- 10 cm, with larger magnitude differences found along the Amundsen-Bellingshausen coastline and off the peninsula in the western Weddell Sea. The mean difference between the two (CryoSat-2 – ICESat-2) is 0.5 cm. While Figure 4 is given to show an example month, this pattern of differences is similar in all months when comparing to ICESat-2.

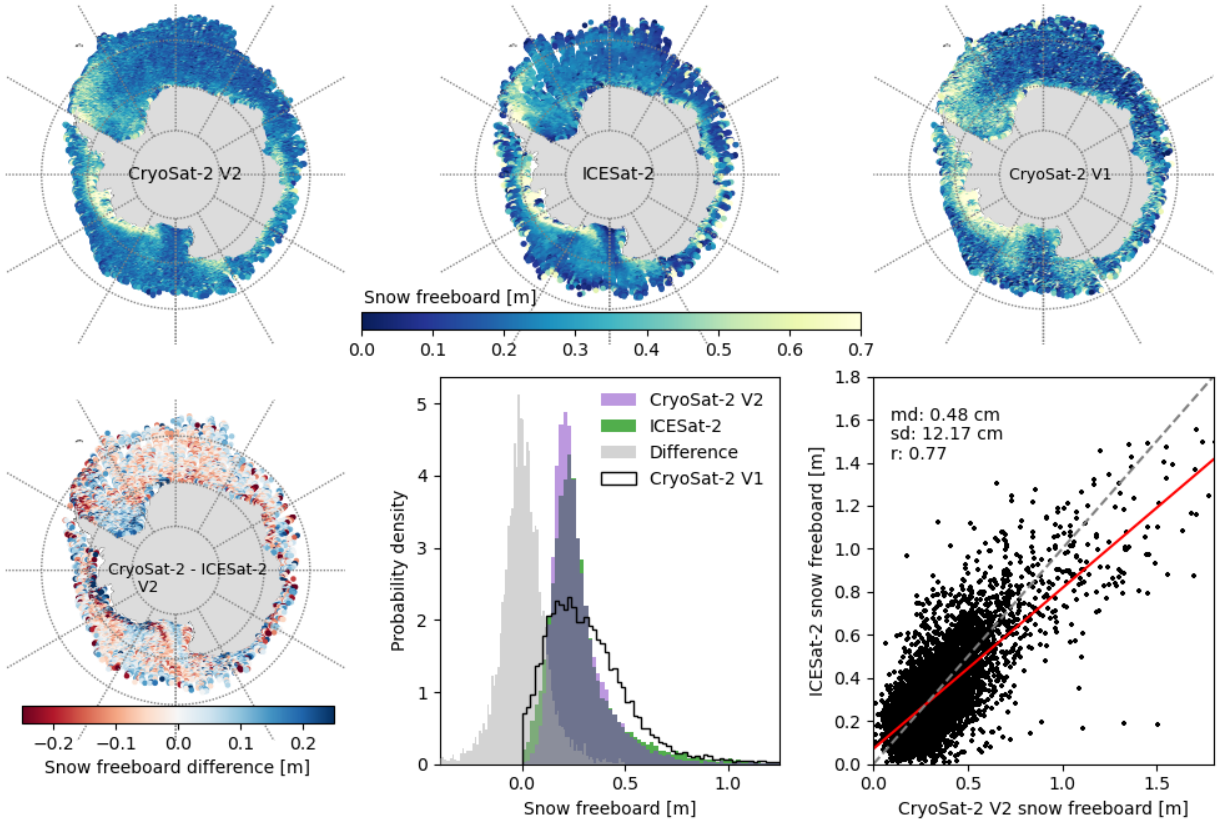

Figure 4. An example monthly comparison between CryoSat-2 and ICESat-2 for September 2020. CryoSat-2 V1 is this month computed by the original method put forth in Fons and Kurtz (2019). The distribution from the V1 map is shown in the black line (lower middle). In the lower right, the dashed line is the 1:1 line, while the red line is the linear best fit.

The original (V1) processing from Fons and Kurtz (2019) was run for this month as well, shown in the top right plot of Figure 4. While a similar spatial pattern of snow freeboard and similar percentage of good fits between V1 and V2 exist, there tend to be thicker freeboards in more of the Weddell Sea and in the Eastern Ross Sea in V1. Additionally, there is more "speckle" in the freeboard pattern from V1 as compared to V2, as the snow freeboard varies more in V1 over a given area. The V1 distribution is broader with a higher spread than the narrower V2 and ICESat-2 distributions, though the modes of all three are similar. It is clear that the improvements made to create the V2 algorithm have a large impact on the freeboard retrievals, leading to better agreement with ICESat-2.

The freeboard distributions from ICESat-2 (green) and CryoSat-2 V2 (purple) for all months of overlapping operation are given in Figure 5. One can see the seasonal evolution in the freeboard distribution, from the broader distributions of Austral summer to the narrower distributions skewed to lower freeboards of the Austral winter. There are consistently more grid cells in the CryoSat-2 data than in the ICESat-2, brought on by data loss due to clouds that attenuate the laser beam but do not impact radar pulses. In general, the distributions given by the two sensors are quite similar, with some systematic differences found in each month, discussed below. The monthly mean freeboard values given by the vertical lines are overall very similar

between CryoSat-2 and ICESat-2, with the exception of larger differences of means in Austral fall months, up to 9 cm in March 2020. The monthly mean differences range from -2.9 to 6.6 cm between CryoSat-2 and ICESat-2, with the standard deviation of differences ranging from 10.8 to 16.8 cm. Correlation coefficients range from 0.57 in January 2020 to 0.80 in September 2019.

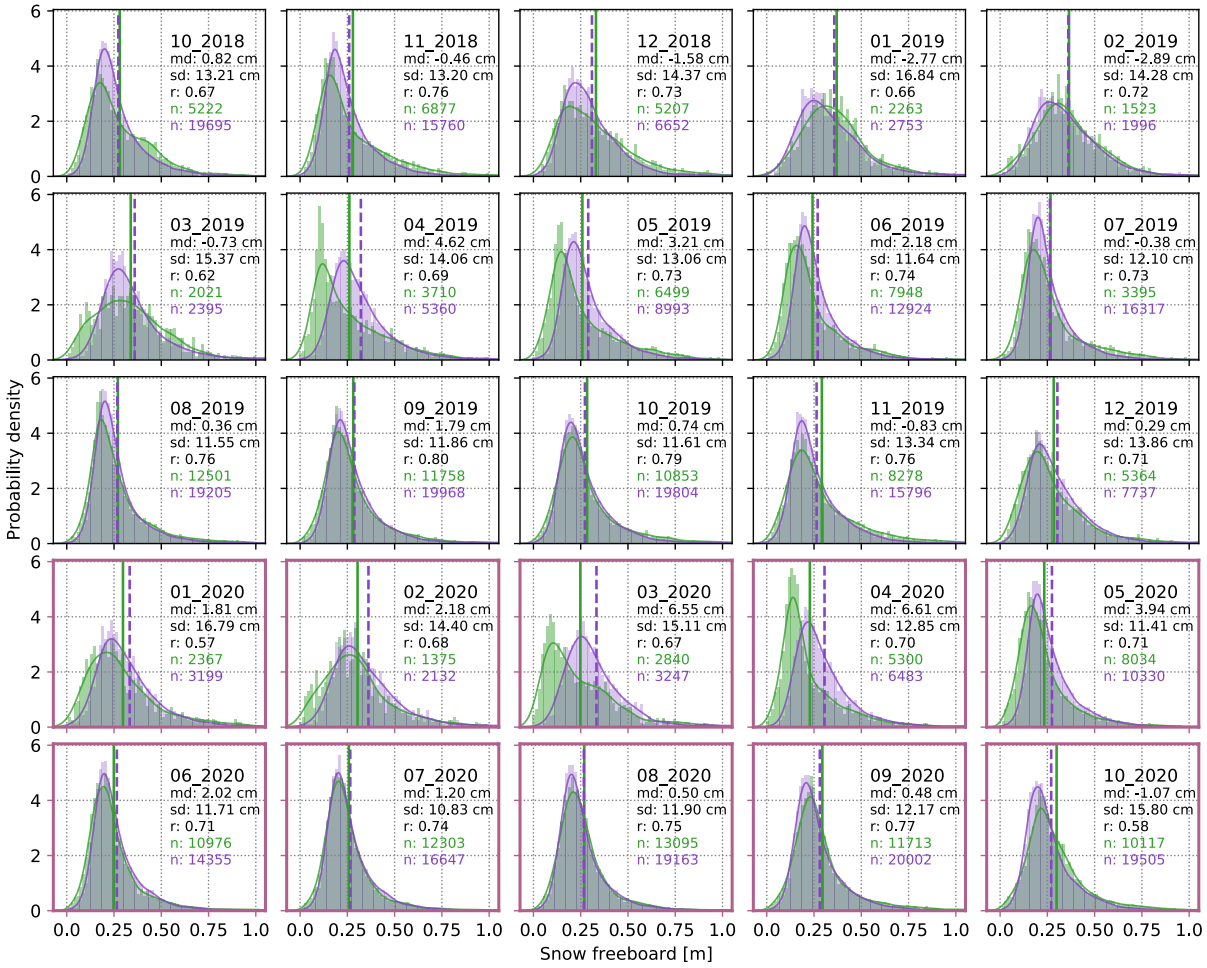

Figure 5. Snow freeboard density histograms and PDFs from CryoSat-2 V2 (purple) and ICESat-2 (green) for October 2018 to October 2020. Mean values are shown by the vertical lines. Plots from 2020, where no coincident ICESat-2 data are included in the initialization, are bordered in red.

In most months shown in Figure 5, ICESat-2 records a greater frequency of thinner (10-15 cm and below) and thicker (50 cm and greater) freeboards. Inversely, CryoSat-2 records a greater probability of "average" (20 to 30 cm) freeboard compared to ICESat-2. In the Austral fall, mainly in March and April 2019 and 2020, the shape of the distributions are most dissimilar, with ICESat-2 skewed to thinner freeboards compared to CryoSat-2. These differences in the freeboard distributions are discussed in later sections.

4.3 Snow freeboard variability

Here, we investigate differences in the monthly mean snow freeboards between CryoSat-2 and ICESat-2 and variability in the measurements. Averaging all years of data for each calendar month yields a mean annual cycle (for the two years October 2018-October 2020), given in Figure 6a. Both CryoSat-2 and ICESat-2 exhibit similar shapes in the cycle, with the most notable difference being the more gradual monthly changes in CryoSat-2 freeboards during the Austral fall months compared to ICESat-2. To get a sense of the grid cell variability in the freeboard measurements from both instruments, we compute the standard deviation of all snow freeboard measurements (σ_{fb}) in each 25 km grid cell for a given month. For ICESat-2, σ_{fb} is around 5 cm basin-wide, but ranges monthly from ~3.4 (June) to ~7.5 cm (February). For CryoSat-2, σ_{fb} is smaller – around 3 cm basin-wide – and ranges between 2.5 (July) and 3.7 cm (February). These values are given as the shading in Figure 6a.

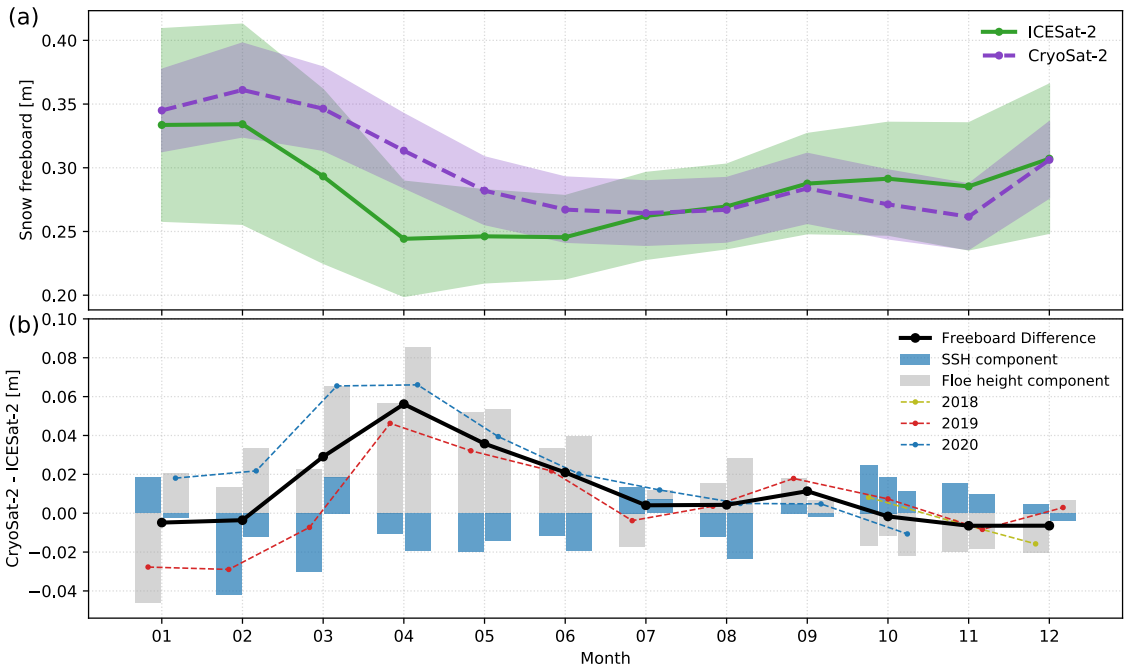

Figure 6. (a) Monthly basin-wide mean snow freeboard from ICESat-2 (green) and CryoSat-2 V2 (purple) averaged from October 2018 to October 2020. Shaded region gives the basin-average standard deviation of freeboard measurements in each grid cell, σ_{fb}. (b) Snow freeboard difference (CryoSat-2 V2 minus ICESat-2) for each year 2018 – 2020 and the total average. Freeboard differences are broken into the SSH (blue) and elevation (grey) components (bars) where the left-most bar in each month represents the earlier year of data for that month (2019 in January -September, 2018 in October – December).

The monthly mean freeboard differences (CryoSat-2 – ICESat-2) are shown in Figure 6b, where the dashed lines indicate the mean freeboard differences from each year, and the solid black line indicates the 2018-2020 mean freeboard difference for each calendar month. As was also shown in Figure 5, the largest differences occur in Austral fall, with CryoSat-2 recording as much as ~6 cm thicker snow freeboards compared to ICESat-2. In other months, differences fall

between +/- 1cm, which is mostly in part to offsetting, larger differences in the SSH and floe elevation components. The variability in differences between individual years is largest in January through March (around 5 cm) but is around 2 cm in all other months.

The mean freeboard differences in Figure 6b are broken down into the contributions from the SSH difference and floe height elevation difference. These components are given as bars where each two-colored bar represents a different year (earlier year of data for a given month is on the left). Since the mean freeboard difference is the sum of the elevation plus the SSH components, the elevation difference can be greater than the freeboard difference when the SSH difference is negative (and vice versa). The SSH difference between CryoSat-2 and ICESat-2 is typically within +/- 2 cm, reaching as much as -4 cm in February 2019. The floe elevation difference is typically largest in Austral fall, where it reaches over 8 cm, and is smaller in later months of the year. The elevation difference dominates the large freeboard differences found in Austral fall. A discussion on potential sources of these differences is given in the following section.

4.4 Potential sources of Austral fall differences

The increase in snow freeboard differences between CryoSat-2 and ICESat-2 during Austral fall could be due to a number of factors. Here, we explore a few potential drivers: the presence of new ice growth, a higher percentage of mixed-surface types during these months, and the fixed snow surface backscatter coefficient used in the retrieval.

Figure 7 compares CryoSat-2 and ICESat-2 snow freeboards for March 2020, when some of the largest differences were present, and relates these differences to new ice formation. The mean basin-wide difference for this month is 6.6 cm, with the spatial pattern of differences (CryoSat-2 minus ICESat-2) shown in Figure 7a. The largest positive differences are collocated with areas of positive sea ice concentration change (7b) as well as areas of new growth (grid cells that were <50% concentration in February 2020 and ≥50% concentration in March 2020, Figure 7c). This is further shown by the differences in individual regions, given in Figure 7d-i: regions in which there are higher percentages of new growth grid cells (Eastern Weddell, Indian, and Ross sectors) tend to show greater positive freeboard differences, while those with fewer new growth grid cells (Western Weddell, Amundsen-Bellingshausen, and Pacific sectors) tend to show smaller mean snow freeboard differences. One explanation for the larger, positive bias over new ice growth could be the initialization of the snow depth parameter in the waveform model. The waveform model is always initialized with a snow layer and therefore could be fit to the CryoSat-2 data with a non-zero output snow depth parameter even if the ice is snow-free. Around 35% of new ice grid cells in March 2020 are initialized with a snow depth greater than

30 cm, meaning the retrieval process could not output a zero snow depth given the fitting bounds, potentially explaining the snow freeboard overestimation compared to ICESat-2.

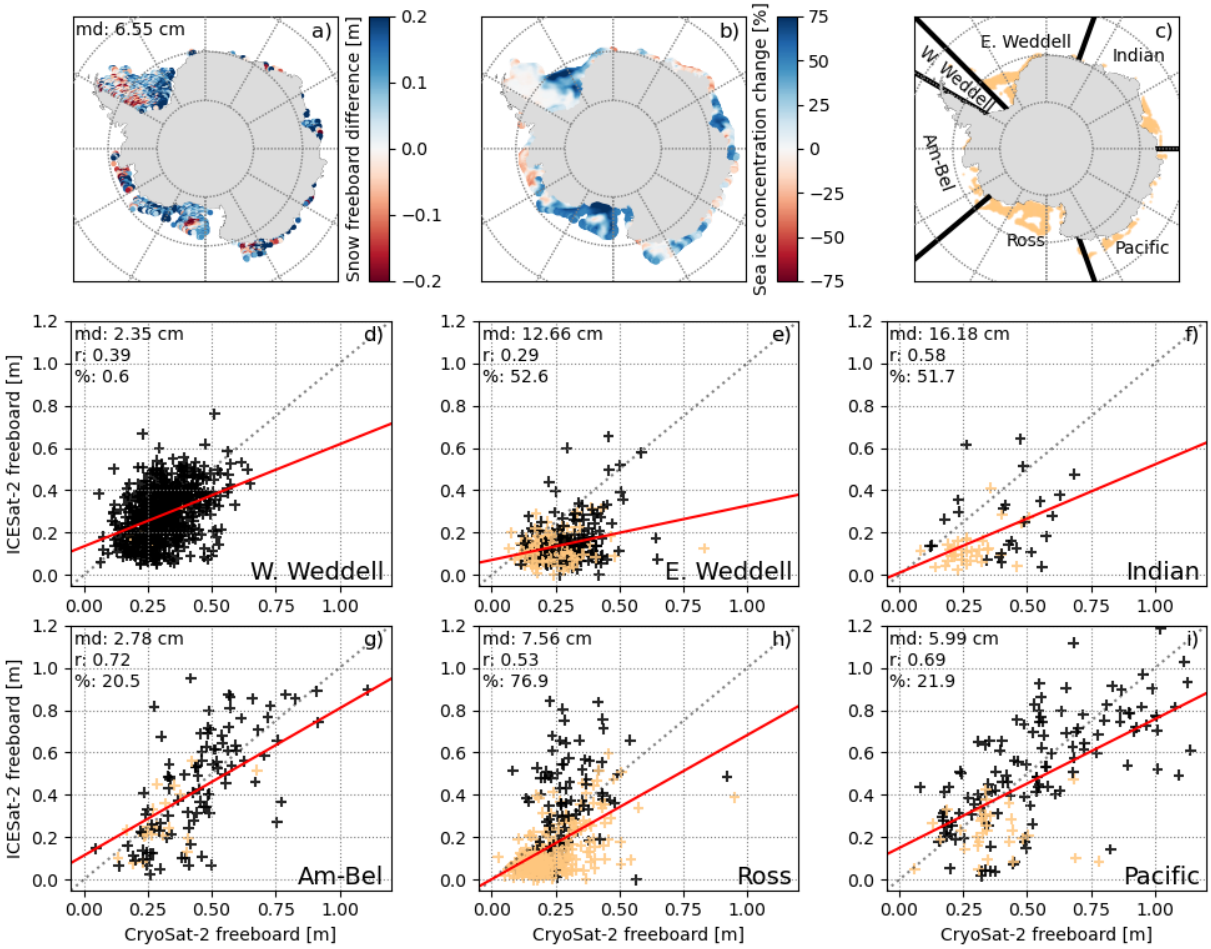

Figure 7. (a) March 2020 snow freeboard difference CryoSat-2 minus ICESat-2. (b) Change in sea ice concentration from February to March 2020. (c) Areas of new ice growth, defined as 25 km grid cells in which ice concentration was <50% in February 2020 and ≥50% in March 2020, and longitudinally-demarcated regions shown in scatter plots below. (d-i) regression between CryoSat-2 (x-axis) and ICESat-2 snow freeboards (y-axis) for each region given in (c), with the mean difference (md), correlation coefficient (r), and percentage of grid cells coming from new ice (%) shown. Orange points indicate grid cells containing new ice as shown in (c). Dashed line is the 1:1 line, while red line gives the linear fit.

A related impact of new ice growth is the potential for more mixed surfaces within the CryoSat-2 footprint. In March and April 2019 and 2020, the percentage of CryoSat-2 waveforms classified as 'mixed' ranges from 12.1 to 12.3%, while in all other months the mixed waveform percent ranges from 9.8 to 11.8% basin-wide. The higher percentage of mixed-surface returns could contribute to differences observed here, as the laser and radar pulses respond differently to mixed surfaces (explained in section 5).

Another cause of the difference observed could be the static backscatter terms used in the waveform model. Very likely, the actual snow surface backscatter changes regionally and seasonally, and using a fixed value could lead to potentially large freeboard biases. Figure 8 shows the snow freeboard sensitivity to varying snow surface backscatter values, both at the single-waveform scale (8a) and over the monthly grid (8b) for April 2020, another month when some of the largest difference were present. Varying the snow surface backscatter between -20 and 20 dB can lead to changes as large as ~30 cm in the retrieved snow freeboard from a single example waveform. This study uses a snow surface backscatter of 0 dB, shown by the purple line and histogram in Figure 8. When this value is increased to equal the ice surface backscatter (8 dB) the retrieved snow freeboard becomes almost 5 cm thinner basin-wide compared to the 0 dB snow surface backscatter (Figure 8b). This leads to a lower mean difference compared to ICESat-2 of 1.7 cm. Decreasing the backscatter to -8 dB (blue line and histogram in Figure 8) results in thicker freeboards basin-wide and a difference from ICESat-2 of over 15 cm.

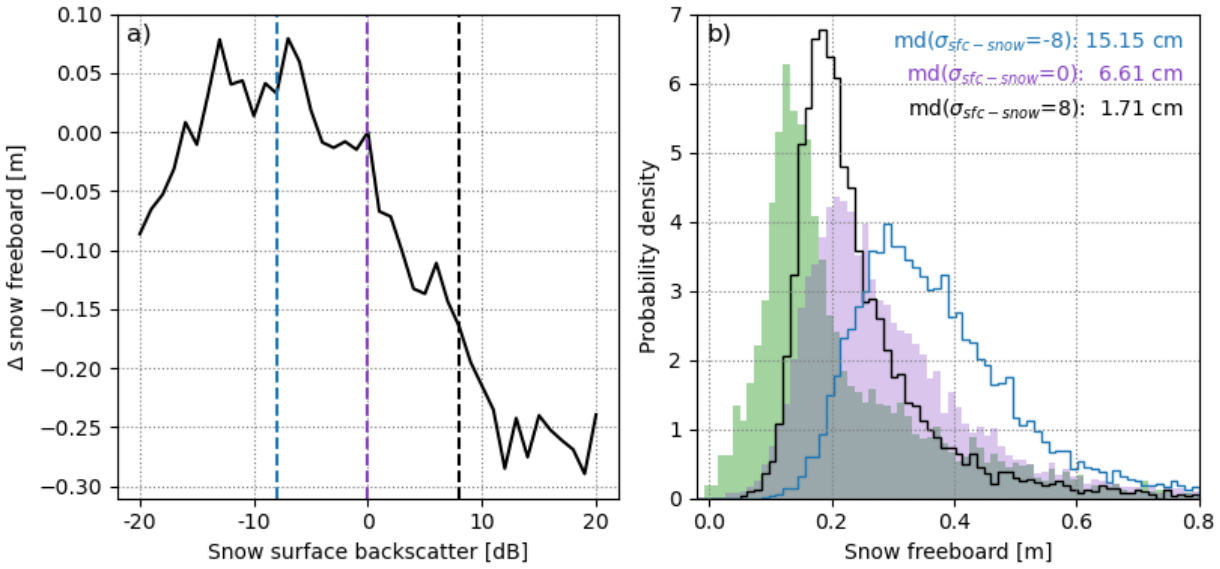

Figure 8. (a) Sensitivity of snow freeboard to the snow surface backscatter value used for an example waveform with a 25 cm initial-guess snow depth. Purple line gives the value used in this study (0 dB) while black and blue lines give the test values (8 and -8 dB, respectively) used in (b). (b) April 2020 snow freeboard distribution from ICESat-2 (green), CryoSat-2 $\sigma^0_{sfc\text{-}snow}$= 0 dB (purple), 8 dB (black), and -8 dB (blue). The mean difference (md) CryoSat-2 minus ICESat-2 is given for all values of $\sigma^0_{sfc\text{-}snow}$.

It is clear that this algorithm shows less agreement with ICESat-2 over new ice growth, and that retrieved freeboards are sensitive to the backscatter values used. While seasonally and regionally-varying backscatter values could help to improve the retrievals in fall months, the lack of knowledge of how backscatter values vary over Antarctic sea ice prevents assigning seasonally-varying quantities. New Ku-band backscatter data from field-based sea ice studies – such as that from Stroeve et al. (2020) – could be incorporated into this algorithm as a future improvement.

5 Discussion

Results from the V2 algorithm show substantial improvement over the V1 algorithm and better agreement with ICESat-2 snow freeboards, especially in the monthly comparisons. This agreement is particularly encouraging for the monthly comparisons in 2020 when no ICESat-2 data were included in the model fitting initialization. The along-track comparisons are promising but stronger conclusions are hard to draw due to the time difference between satellite overlaps. Despite the similarity, there still exist differences in the retrieved freeboards brought on by inherent sampling discrepancies between the satellites, discussed herein.

Comparing the along-track freeboards in Figure 3, it is likely that differences between CryoSat-2 V2 and ICESat-2 arise from two major sources: the time delay between satellite overlaps and the sampling (both geometry and frequency) differences between the instruments. As mentioned in section 4.1, the time delay between the satellite overpasses in the Southern Ocean is at minimum three hours. In the locations of the two overlaps in Figure 3, the monthly mean sea ice drift can reach upwards of 10 km per day (Kwok et al., 2017), meaning that the two satellites could be sampling entirely different sea ice. The location of the 2018 overlap in the Amundsen Sea typically experiences faster sea ice drift than the location of the 2019 overlap in the near-coastal Weddell Sea (Kwok et al., 2017), which could explain the higher correlations observed in 2019. Additionally, the 2019 profile records on average ~11 consecutive CryoSat-2 floe points between lead points (a proxy for floe size), while the 2018 profile records ~7 consecutive floe points between each lead measurement on average. This difference could suggest larger floes during the 2019 profile compared to 2018, which could help to explain the higher correlations.

In addition to the time offsets, the large sampling differences – both geometric and frequency-related – likely also contribute to the differences in freeboards observed here. Sea ice surface features can vary greatly over small areas, and the CryoSat-2 SAR/SARIn footprint – with an area over 6,000 times larger than an ICESat-2 footprint – will sample much more of the surface per shot and therefore sample different features with varying elevations and freeboards (Giles et al., 2007). Due to this footprint size difference, the small difference in mean freeboards and similar distributions (especially in 2018) is encouraging, despite the variability in the along-track shot-to-shot freeboard profiles. Additionally, the sampling frequency combined with footprint size limit CryoSat-2 SAR data to approximately 2.6 measurements per along-track kilometer, while ICESat-2 is able to record upwards of ~50 measurements per kilometer, depending on the photon rate and resultant segment length. This higher number of samples provides an enhanced resolution along the surface and could allow ICESat-2 to better capture the thickest and thinnest freeboards observed in the profiles.

The mean snow freeboard differences (Figure 6) display an overestimation of the snow freeboard by CryoSat-2 in Austral fall when compared to ICESat-2. This discrepancy is dominated more by the elevation retrieval and less from the SSH, and we estimate that this difference arises from complications due to new ice growth as well as the static backscatter initialization used in the waveform-fitting model. As mentioned above, we initialize the snow depth parameter using snow freeboard data and apply the zero-ice-freeboard assumption (Kurtz & Markus, 2012, sec. 3.5). This assumption is likely an overestimate of the snow depth on Antarctic sea ice (Kwok & Kacimi, 2018), and a possible contributor to the positive differences observed here. Since the largest differences occur over new ice growth (Figure 7), it is probable that initializing a snow depth using this method when no snow layer may exist could lead to the observed freeboard overestimation. Clearly, the zero ice freeboard assumption may not be valid

for all seasons and regions, enhancing uncertainty in the retrieved freeboards. In the absence of reliable pan-Antarctic snow depth estimates, however, this initialization is used until more snow depth data are made available.

The geometric sampling discrepancy discussed above could also contribute to the seasonal freeboard differences observed (Figure 6). Tilling et al. (2019) found that Arctic freeboard data from the larger-footprint Envisat displayed a thick bias compared to the smaller-footprint CryoSat-2, that was attributed to enhanced off-nadir ranging to leads in less-consolidated ice regions. This effect would theoretically be present when comparing CryoSat-2 and ICESat-2, where the difference in footprint size is greater than that of CryoSat-2 and Envisat. Paul et al. (2018, figure 11) also compared CryoSat-2 and Envisat freeboards but in the Antarctic, and showed similar differences in freeboard distributions to the ones shown in Figure 5. In both cases, the smaller footprint satellite (CryoSat-2 in Paul et al. (2018) and ICESat-2 here) tended to have broader freeboard distributions while the larger-footprint satellite (Envisat in Paul et al. (2018) and CryoSat-2 here) showed taller, narrower distributions. Even the seasonality of the distribution differences closely aligns between Figure 5 and Paul et al. (2018), where discrepancies are found to be largest in Austral fall. This finding leads us to hypothesize that the differing footprint sizes may contribute to the differences in freeboard distributions shown. More work is needed, however, to quantify the geometric sampling discrepancies and determine the amount that they contribute to the differences in the freeboard distributions.

It is important to note that the comparisons shown in Tilling et al. (2019) and Paul et al. (2018) compare sensors of the same wavelength, while CryoSat-2 and ICESat-2 are entirely different in their altimeter concept and operating frequencies. It is likely that scattering differences between radar and laser also contribute to the discrepancies observed here. Each radar pulse responds to the sea ice surface differently than that from a laser, which is especially true over mixed sea ice and open water surfaces. In footprints containing both sea ice and leads, a radar pulse can get overwhelmed by the strong specular return from the water while the laser can either record a drop or a rise in the surface photon rate depending on the roughness of the water surface (Kwok et al., 2020; Ricker et al., 2014; Tilling et al., 2017). Additionally, the Ku-band backscatter coefficient varies non-linearly across heterogeneous surfaces (Landy et al., 2019), which means that a radar return does not represent an average of the surfaces in the footprint, but is instead weighted based on the roughness of the surface and features present. The fact that March and April were found to have slightly higher percentages of mixed surface types compared to the rest of the year could suggest that these mixed surfaces contribute to the differences observed. More ground-based studies of laser and radar scattering over sea ice, similar to Stroeve et al. (2020), would be useful to better quantify the potential uncertainty brought on by the footprint-scale scattering of these sensors, which could enable better comparisons.

6 Conclusions and future work

In this work, we have outlined improvements made to the CryoSat-2 waveform-fitting retrieval algorithm put forth in Fons and Kurtz (2019) and showcased first comparisons of the snow freeboard retrievals to ICESat-2 data in the Southern Ocean. Some significant changes were implemented that improved the physical representativeness of the model, reduced the potential for anomalous convergence on local minima, and increased processing efficiency. These V2 improvements were motivated by recent publications (such as Landy et al. (2020) and Mallett et al. (2020)). We ran this improved algorithm on all CryoSat-2 data from October 2018

to October 2020 in order to compare with new snow freeboard data obtained from NASA's ICESat-2.

Our results showed 2018-2020 monthly mean differences between these CryoSat-2 snow freeboard retrievals and ICESat-2 ATL10 data ranging seasonally from -0.6 to 5.6 cm. When comparing coincident along-track profiles and individual monthly grids, differences ranged from 0.3 to 7.6 cm and -2.9 to 6.6 cm, respectively. We find that snow freeboard distributions between the two instruments are comparable in shape, but hypothesize that differences could arise from geometric sampling and sensor frequency discrepancies. These differences are enhanced in Austral fall, matching what was found by Paul et al. (2018) comparing Envisat and CryoSat-2. More work is needed to discern the exact role that the new ice and thin snow depths found during these months play in the observed freeboard overestimation, and how the initialized zero ice freeboard assumption and wavelength discrepancies between these two sensors may also contribute. In-situ data freeboard data – which is currently lacking for this time period - would also help to better evaluate both sensors.

In order to more accurately assess the retrievals and compare snow freeboard measurements from these two sensors, more - and longer - orbital overlaps with a time delay closer to zero would be beneficial. These overlaps could also help in estimating systematic uncertainty in the CryoSat-2 retrievals, which is challenging due to a considerable lack in ground truth data from Antarctic sea ice. This idea of generating more overlaps between CryoSat-2 and ICESat-2 is the premise behind the CRYO2ICE campaign, which is currently providing near-coincident overlaps in the Arctic. However, since the orbital realignment in late July 2020, no CryoSat-2 and ICESat-2 overlaps (as defined above) have occurred over sea ice in the Southern Hemisphere as of December 2020. To better facilitate sea ice research in the Southern Ocean, it would be useful to adjust the orbital configuration to optimize for the Southern Hemisphere, as proposed by the CRYO2ICE project (ESA, 2018).

Moving forward, we hope this work can be useful for deriving new estimates of sea ice snow freeboard in the Southern Ocean for the length of the CryoSat-2 mission, which do not currently exist. A CryoSat-2 snow freeboard time series could be reconciled with that from ICESat and ICESat-2 to create a more than 17-year record of Antarctic snow freeboard. Further exploration and validation into the snow depth parameter produced in this forward model output is necessary, but, combined with these or other estimates of freeboard, could enable Antarctic sea ice thickness calculations from CryoSat-2.

Acknowledgements

We would like to thank the members of both the CryoSat-2 and ICESat-2 projects for their efforts in developing and disseminating quality altimetry data. Additionally, we would like to thank Stefan Hendricks and an anonymous reviewer for their comments that helped to improve this manuscript.

Data availability

CryoSat-2 level 1-B data were obtained through the CryoSat-2 Science Server at https://science-pds.cryosat.esa.int. The gridded and along-track CryoSat-2 snow freeboard estimates derived in this study are available on Zenodo: https://doi.org/10.5281/zenodo.4565587. ICESat-2 freeboard data (ATL10) are available through NSIDC at https://nsidc.org/data/atl10. Orbit files for CryoSat-2 and ICESat-2 used in finding near-coincident overlaps can be found at

ftp://calval-pds.cryosat.esa.int/ and https://icesat-2.gsfc.nasa.gov/science/specs, respectively. ICESat freeboard data used in the model initialization can be found at https://earth.gsfc.nasa.gov/cryo/data/antarctic-sea-ice-thickness

References

Arthern, R. J., Wingham, D. J., & Ridout, A. L. (2001). Controls on ERS altimeter measurements over ice sheets: Footprint-scale topography, backscatter fluctuations, and the dependence of microwave penetration depth on satellite orientation. *Journal of Geophysical Research: Atmospheres*, *106*(D24), 33471–33484. https://doi.org/10.1029/2001JD000498

Beaven, S. G., Lockhart, G. L., Gogineni, S. P., Hossetnmostafa, A. R., Jezek, K., Gow, A. J., et al. (1995). Laboratory measurements of radar backscatter from bare and snow-covered saline ice sheets. *International Journal of Remote Sensing*, *16*(5), 851–876. https://doi.org/10.1080/01431169508954448

Cavalieri, D. J., Parkinson, C. L., Gloersen, P., & Zwally, H. J. (1996). Sea Ice Concentrations from Nimbus-7 SMMR and DMSP SSM/I-SSMIS Passive Microwave Data, Version 1. Boulder, Colorado USA. https://doi.org/10.5067/8GQ8LZQVL0VL

Comiso, J. C. (2017). Bootstrap Sea Ice Concentrations from Nimbus-7 SMMR and DMSP SSM/I-SSMIS, Version 3. Boulder, Colorado USA: NASA National Snow and Ice Data Center Distributed Active Archive Center. https://doi.org/10.5067/7Q8HCCWS4I0R

Connor, L. N., Laxon, S. W., Ridout, A. L., Krabill, W. B., & McAdoo, D. C. (2009). Comparison of Envisat radar and airborne laser altimeter measurements over Arctic sea ice. *Remote Sensing of Environment*, *113*(3), 563–570. https://doi.org/10.1016/j.rse.2008.10.015

European Space Agency. (2019). L1b SAR Precise Orbit. Baseline D. https://doi.org/10.5270/CR2-2cnblvi

European Space Agency. (2018). *Introduction to CryoSat-2 ICESat-2 Resonant Orbits*. Retrieved from https://earth.esa.int/eogateway/missions/cryosat/cryo2ice

European Space Agency. (2019). L1b SARIn Precise Orbit. Baseline D. https://doi.org/10.5270/CR2-u3805kw

European Space Agency. (2019). *CryoSat-2 Product Handbook: Baseline D 1.1*. Retrieved from https://earth.esa.int/documents/10174/125272/CryoSat-Baseline-D-Product-Handbook

Fons, S. W., & Kurtz, N. T. (2019). Retrieval of snow freeboard of Antarctic sea ice using waveform fitting of CryoSat-2 returns. *The Cryosphere*, *13*(3), 861–878. https://doi.org/10.5194/tc-13-861-2019

Giles, K. A., Laxon, S. W., Wingham, D. J., Wallis, D. W., Krabill, W. B., Leuschen, C. J., et al. (2007). Combined airborne laser and radar altimeter measurements over the Fram Strait in May 2002. *Remote Sensing of Environment*, *111*(2), 182–194. https://doi.org/10.1016/j.rse.2007.02.037

Hendricks, S.; Paul, S.; Rinne, E. (2018). ESA Sea Ice Climate Change Initiative (Sea_Ice_cci): Southern hemisphere sea ice thickness from the CryoSat-2 satellite on a monthly grid (L3C), v2.0. *Centre for Environmental Data Analysis*. https://doi.org/10.5285/48fc3d1e8ada405c8486ada522dae9e8

Kacimi, S., & Kwok, R. (2020). The Antarctic sea ice cover from ICESat-2 and CryoSat-2: freeboard, snow depth, and ice thickness. *The Cryosphere*, *14*, 4453–4474. https://doi.org/10.5194/tc-14-4453-2020

Kern, S., Ozsoy-Çiçek, B., & Worby, A. (2016). Antarctic Sea-Ice Thickness Retrieval from ICESat: Inter-Comparison of Different Approaches. *Remote Sensing*, *8*(7), 538. https://doi.org/10.3390/rs8070538

Kurtz, N. T., Galin, N., & Studinger, M. (2014). An improved CryoSat-2 sea ice freeboard retrieval algorithm through the use of waveform fitting. *Cryosphere*, *8*(4), 1217–1237. https://doi.org/10.5194/tc-8-1217-2014

Kurtz, N. T., & Markus, T. (2012). Satellite observations of Antarctic sea ice thickness and volume. *Journal of Geophysical Research: Oceans*, *117*(8), n/a-n/a. https://doi.org/10.1029/2012JC008141

Kwok, R. (2014). Simulated effects of a snow layer on retrieval of CryoSat-2 sea ice freeboard. *Geophysical Research Letters*, *41*(14), 5014–5020. https://doi.org/10.1002/2014GL060993

Kwok, R., & Cunningham, G. F. (2015). Variability of Arctic sea ice thickness and volume from CryoSat-2. *Philosophical Transactions of the Royal Society A: Mathematical, Physical and Engineering Sciences*, *373*(2045), 20140157. https://doi.org/10.1098/rsta.2014.0157

Kwok, R., Cunningham, G. F., Markus, T., Hancock, D. W., Morison, J. H., Palm, S. P., et al. (2020). ATLAS/ICESat-2 L3A Sea Ice Height (ATL07), Version 3. *NASA National Snow and Ice Data Center Distributed Active Archive Center*. https://doi.org/10.5067/ATLAS/ATL10.003

Kwok, R., Markus, T., Kurtz, N. T., Petty, A. A., Neumann, T. A., Farrell, S. L., et al. (2019). Surface Height and Sea Ice Freeboard of the Arctic Ocean From ICESat-2: Characteristics and Early Results. *Journal of Geophysical Research: Oceans*, *124*(10), 6942–6959. https://doi.org/10.1029/2019JC015486

Kwok, R., Cunningham, G. F., Hancock, D. W., Ivanoff, A., & Wimert, J. T. (2020). *ICESat-2 Algorithm Theoretical Basis Document for Sea Ice Products (ATL07/ATL10) Release 003*

ICE, CLOUD, and Land Elevation Satellite (ICESat-2) Project Algorithm Theoretical Basis Document (ATBD) For Sea Ice Products. https://doi.org/10.5067/UAZPI91070H4

Kwok, R., & Kacimi, S. (2018). Three years of sea ice freeboard, snow depth, and ice thickness of the Weddell Sea from Operation IceBridge and CryoSat-2. *The Cryosphere*, *12*(8), 2789–2801. https://doi.org/10.5194/tc-12-2789-2018

Kwok, R., Pang, S. S., & Kacimi, S. (2017). Sea ice drift in the Southern Ocean: Regional patterns, variability, and trends. *Elementa*, *5*. https://doi.org/10.1525/elementa.226

Landy, J. C., Petty, A. A., Tsamados, M., & Stroeve, J. C. (2020). Sea Ice Roughness Overlooked as a Key Source of Uncertainty in CryoSat-2 Ice Freeboard Retrievals. *Journal of Geophysical Research: Oceans*, *125*(5). https://doi.org/10.1029/2019JC015820

Landy, J. C., Tsamados, M., & Scharien, R. K. (2019). A Facet-Based Numerical Model for Simulating SAR Altimeter Echoes from Heterogeneous Sea Ice Surfaces. *IEEE Transactions on Geoscience and Remote Sensing*, *57*(7), 4164–4180. https://doi.org/10.1109/TGRS.2018.2889763

Laxon, S. W., Giles, K. A., Ridout, A. L., Wingham, D. J., Willatt, R., Cullen, R., et al. (2013). CryoSat-2 estimates of Arctic sea ice thickness and volume. *Geophysical Research Letters*, *40*(4), 732–737. https://doi.org/10.1002/grl.50193

Laxon, S., Peacock, H., & Smith, D. (2003). High interannual variability of sea ice thickness in the Arctic region. *Nature*, *425*(6961), 947–950. https://doi.org/10.1038/nature02050

Lee, S., Im, J., Kim, J., Kim, M., Shin, M., Kim, H., & Quackenbush, L. (2016). Arctic Sea Ice Thickness Estimation from CryoSat-2 Satellite Data Using Machine Learning-Based Lead Detection. *Remote Sensing*, *8*(9), 698. https://doi.org/10.3390/rs8090698

Li, H., Xie, H., Kern, S., Wan, W., Ozsoy, B., Ackley, S., & Hong, Y. (2018). Spatio-temporal variability of Antarctic sea-ice thickness and volume obtained from ICESat data using an innovative algorithm. *Remote Sensing of Environment*, *219*, 44–61. https://doi.org/10.1016/j.rse.2018.09.031

Mallett, R. D. C., Lawrence, I. R., Stroeve, J. C., Landy, J. C., & Tsamados, M. (2020). Brief communication: Conventional assumptions involving the speed of radar waves in snow introduce systematic underestimates to sea ice thickness and seasonal growth rate estimates. *The Cryosphere*, *14*(1), 251–260. https://doi.org/10.5194/tc-14-251-2020

Massom, R. A., Eicken, H., Haas, C., Jeffries, M. O., Drinkwater, M. R., Sturm, M., et al. (2001). Snow on Antarctic sea ice. *Reviews of Geophysics*, *39*(3), 413–445. https://doi.org/10.1029/2000RG000085

761 Meier, W. N., Fetterer, F., & Windnagel, A. K. (2017). Near-Real-Time NOAA/NSIDC Climate
762 Data Record of Passive Microwave Sea Ice Concentration, Version 1.
763 https://doi.org/0.7265/N5FF3QJ6

764 Meredith, M., M. Sommerkorn, S. Cassotta, C. Derksen, A. Ekaykin, A. Hollowed, G. Kofinas,
765 A. Mackintosh, J. Melbourne-Thomas, M.M.C. Muelbert, G. Ottersen, H. Pritchard, and
766 E.A.G. Schuur, (2019). Polar Regions. In: *IPCC Special Report on the Ocean and*
767 *Cryosphere in a Changing Climate* [H.-O. Pörtner, D.C. Roberts, V. Masson-Delmotte, P.
768 Zhai, M. Tignor, E. Poloczanska, K. Mintenbeck, A. Alegría, M. Nicolai, A. Okem, J.
769 Petzold, B. Rama, N.M. Weyer (eds.)]. In press. https://www.ipcc.ch/srocc/chapter/chapter-
770 3-2/

771 Nandan, V., Geldsetzer, T., Yackel, J., Mahmud, M., Scharien, R., Howell, S., et al. (2017).
772 Effect of Snow Salinity on CryoSat-2 Arctic First-Year Sea Ice Freeboard Measurements.
773 *Geophysical Research Letters*, *44*(20), 10,419-10,426.
774 https://doi.org/10.1002/2017GL074506

775 Paul, S., Hendricks, S., Ricker, R., Kern, S., & Rinne, E. (2018). Empirical parametrization of
776 Envisat freeboard retrieval of Arctic and Antarctic sea ice based on CryoSat-2: progress in
777 the ESA Climate Change Initiative. *The Cryosphere*, *12*(7), 2437–2460.
778 https://doi.org/10.5194/tc-12-2437-2018

779 Price, D., Beckers, J., Ricker, R., Kurtz, N., Rack, W., Haas, C., et al. (2015). Evaluation of
780 CryoSat-2 derived sea-ice freeboard over fast ice in McMurdo Sound, Antarctica. *Journal*
781 *of Glaciology*, *61*(226), 285–300. https://doi.org/10.3189/2015JoG14J157

782 Reiser, F., Willmes, S., & Heinemannm Gunther. (2020). A New Algorithm for Daily Sea Ice
783 Lead Identification in the Arctic and Antarctic Winter from Thermal-Infrared Satellite
784 Imagery. *Remote Sensing*, *12*, 1957. https://doi.org/10.3390/rs12121957

785 Ricker, R., Hendricks, S., Helm, V., Skourup, H., & Davidson, M. (2014). Sensitivity of
786 CryoSat-2 Arctic sea-ice freeboard and thickness on radar-waveform interpretation. *The*
787 *Cryosphere*, *8*(4), 1607–1622. https://doi.org/10.5194/tc-8-1607-2014

788 Scagliola, M. (2013). *Advanced Doppler ambiguity resolution strategies for Wave Mode Data:*
789 *CryoSat footprints*. Retrieved from
790 https://earth.esa.int/documents/10174/125271/CryoSat_Footprints_TN_v1.1.pdf

791 Schwegmann, S., Rinne, E., Ricker, R., Hendricks, S., & Helm, V. (2016). About the consistency
792 between Envisat and CryoSat-2 radar freeboard retrieval over Antarctic sea ice. *The*
793 *Cryosphere*, *10*(4), 1415–1425. https://doi.org/10.5194/tc-10-1415-2016

794 Stroeve, J., Nandan, V., Willatt, R., Tonboe, R., Hendricks, S., Ricker, R., Mead, J., Mallett, R.,
795 Huntemann, M., Itkin, P., Schneebeli, M., Krampe, D., Spreen, G., Wilkinson, J., Matero, I.,
796 Hoppmann, M., and Tsamados, M. (2020). Surface-based Ku- and Ka-band polarimetric

radar for sea ice studies. *The Cryosphere*, 14, 4405–4426. https://doi.org/10.5194/tc-14-4405-2020

Tilling, R., Ridout, A., & Shepherd, A. (2019). Assessing the Impact of Lead and Floe Sampling on Arctic Sea Ice Thickness Estimates from Envisat and CryoSat-2. *Journal of Geophysical Research: Oceans*, *124*(11), 7473–7485. https://doi.org/10.1029/2019JC015232

Tilling, R. L., Ridout, A., & Shepherd, A. (2018). Estimating Arctic sea ice thickness and volume using CryoSat-2 radar altimeter data. *Advances in Space Research*, *62*(6), 1203–1225. https://doi.org/10.1016/j.asr.2017.10.051

Virtanen, P., Gommers, R., Oliphant, T. E., Haberland, M., Reddy, T., Cournapeau, D., et al. (2020). SciPy 1.0: fundamental algorithms for scientific computing in Python. *Nature Methods*, *17*(3), 261–272. https://doi.org/10.1038/s41592-019-0686-2

Willatt, R. C., Giles, K. A., Laxon, S. W., Stone-Drake, L., & Worby, A. P. (2010). Field investigations of Ku-band radar penetration into snow cover on antarctic sea ice. *IEEE Transactions on Geoscience and Remote Sensing*, *48*(1), 365–372. https://doi.org/10.1109/TGRS.2009.2028237

Wingham, D. J., Francis, C. R., Baker, S., Bouzinac, C., Brockley, D., Cullen, R., et al. (2006). CryoSat: A mission to determine the fluctuations in Earth's land and marine ice fields. *Advances in Space Research*, *37*(4), 841–871. https://doi.org/10.1016/j.asr.2005.07.027

Zwally, H. J., Yi, D., Kwok, R., & Zhao, Y. (2008). ICESat measurements of sea ice freeboard and estimates of sea ice thickness in the Weddell Sea. *Journal of Geophysical Research: Oceans*, *113*(2). https://doi.org/10.1029/2007JC004284